Acta Polytechnica CTU Proceedings **50**:69–73, 2024
https://doi.org/10.14311/APP.2024.50.0069

Published by the Czech Technical University in Prague

MICROMECHANICAL CHARACTERIZATION OF γ-IRRADIATED CEMENT PASTE EXPOSED TO DIFFERENT RELATIVE HUMIDITY CONDITIONS

Jiří Němeček [1,a,*], Lukáš Procházka[b], Patricie Halodová[b], Jiří Němeček [2,a]

[a] *Czech Technical University in Prague, Faculty of Civil Engineering, Department of Mechanics, Thákurova 7, 166 29 Prague 6, Czech Republic*

[b] *Research Centre Řež, Hlavní 130 Řež, Husinec 250 68, Czech Republic*

[*] corresponding author: jiri.nemecek.1@fsv.cvut.cz

Abstract.

In this study, well-hydrated cement paste samples made from Portland cement CEM I-42.5R were gamma irradiated with a 200 TBq ^{60}Co source, resulting in a total absorbed dose of 13.82 MGy. During irradiation, the samples were stored under specific relative humidity (RH) conditions of 11 %, 33 %, 76 %, 96 %, and water. Grid nanoindentation was performed on polished sample surfaces to assess the nanoindentation Young's modulus of both irradiated and non-irradiated control samples. An increase in Young's modulus by 9.3 % was observed for irradiated samples at low RH (11 %). Samples stored at medium RHs (33 %, 76 %) showed negligible differences in micromechanical properties. However, a significant decrease in Young's modulus, approximately 15 %, was measured for samples stored at high RHs (96 %, water).

Keywords: Cement paste, C–S–H gel, gamma radiation, nanoindentation, relative humidity.

1. Introduction

Concrete in nuclear power plants, used as biological shielding around the active zone, is exposed to radiation and thermal strains [1]. A decrease in mechanical properties, primarily the compressive strength of concrete, was previously reported in [2, 3]. The deterioration is mainly caused by neutron radiation, gamma radiation, drying, and heating [1]. Gamma rays primarily affect the water in Calcium-Silicate-Hydrates (C–S–H) gel due to water radiolysis, causing concrete drying [4]. As most of the studies are conducted on a macro-scale, only a limited amount of research investigates mechanical properties at the micro-scale.

Micromechanical properties of gamma irradiated mortar with an absorbed dose of 12–15 MGy were previously studied by Khmurovska et al. [5]. The samples were exposed to standard relative humidities (RHs) of 40 %–60 %, showing a negligible effect on the Young's modulus of C–S–H phases. Similar findings were presented by Hilloulin et al. [6], but with a significantly lower total absorbed dose of 0.257 MGy. Further, nanoindentation of C–S–H pellets irradiated at 11 % RH was performed by Hunnicutt [7], who irradiated samples up to a dose of 0.784 MGy, reporting again negligible changes in micromechanical properties. However, the authors continued irradiating the pellets with significantly higher doses of 24 MGy and 189 MGy in Baral et al. [8]. The higher dose falls within the range of approximately 100–200 MGy, which is the total gamma dose to which a biological shield is exposed over an 80-year lifespan [9]. In these cases, a significant increase in the nanoindentation Young's modulus by 15 %–25 % was reported for the 189 MGy total dose. It was also reported by Němeček et al. [10] that the RH level in the environment significantly affects the micromechanical properties of 28-day-old cement paste under gamma radiation (absorbed dose 2.88 MGy), especially at low (4–11 %) and high (100 %) RHs.

Therefore, it is evident that during the gamma irradiation of cementitious materials, not only the total absorbed dose but also the RH level and the samples' hydration degree affect the final micromechanical properties. Thus, this study aims to quantify the effect of RH conditions on mature ordinary cement paste exposed to a higher gamma irradiation dose (13.82 MGy).

2. Experiments and methods

2.1. Material and sample preparation

The ordinary cement paste samples were prepared from Portland cement CEM I-42.R (Českomoravský cement, Czech Republic) with a water-to-cement ratio of 0.4. After mixing, the paste was cast into cylindrical molds with a diameter of 27 mm and a height of 70 mm, and then vibrated to remove entrapped air. The samples were demolded after 1 day and placed

[1] Postdoctoral researcher at Czech Technical University in Prague, ORCID: 0000-0002-5635-695X.

[2] Professor at Czech Technical University in Prague, ORCID: 0000-0002-3565-8182.

Label	11	33	76	96	W
RH (%)	11	33	76	96	100
Salt	LiCl	$MgCl_2$	NaCl	KNO_3	–
Other	–	–	–	–	water

Table 1. Labeling and summary of conditions used to control RH.

in a 1 % limewater solution for 20 months, representing fully hydrated samples with degree of hydration (DoH) estimated as 0.88 based on the Cemhyd3D calculation [11]. This high DoH was chosen to minimize changes due to varying storage conditions during one year of gamma irradiation. Subsequently, the samples were cut into smaller cylinders, 20 mm thick, and further placed into plastic containers with five different RH (11 %, 33 %, 76 %, 96 %, and 100 %) conditions. Four of these conditions were created using salt-saturated solutions, while the fifth container was filled with limewater, where the samples were originally stored. The details about the RH conditions and the salts used are provided in Table 1.

2.2. Gamma irradiation

The containers with samples were gamma irradiated using a ^{60}Co radiation source in the Gamma Radiation Facility of the Research Centre Řež, Czech Republic. The average dose rate ranged from 0.675 to 1.890 kGy h^{-1}. The samples were irradiated (IR) for 341 days and absorbed a total dose of 13.82 MGy. Simultaneously, non-irradiated (Non-IR) containers were left under the same RH conditions. The plastic containers were replaced every two months to ensure stable RH conditions throughout the irradiation period [10].

2.3. Sample surface polishing

After the gamma irradiation experiment, all samples were removed from the containers and dried for 3 days at 50 °C to prepare them for polishing. DoH for samples below 76 % RH remain 0.88, while those stored at 96 % RH and 100 % RH showed only a minimal increase of DoH, estimated as 0.90. The dried samples were then polished using silicon carbide papers in the following sequence: #1200 grit for 10 s, #2000 grit for 60 s, and #4000 grit for 200 s. Between each step, the samples were placed in an ultrasonic cleaner with alcohol for 60 s to remove any free particles [12]. The surface roughness of the samples, characterized by the root-mean-square (RMS) parameter, was 41 ± 7 nm on 55×55 µm^2, which is acceptable for nanoindentation with ∼200 nm deep indents.

2.4. Nanoindentation

The nanoindentation was performed with a Hysitron TI-980 Triboindenter equipped with a Berkovich diamond tip. On each sample, ten grids of 22×22 indents were conducted using the accelerated property mapping mode (XPM). The separation between individual indents was set to 2.5 µm to provide high spatial resolution and avoid interaction between indents. A numerical study by Phani and Oliver [13] showed that the safe indentation distance is 10 times the indentation depth. Since our indentations reach depths of up to 200 nm, the 2.5 µm separation falls within the safe range. A total of 484 indents were performed. The load function was selected as trapezoidal, consisting of linear loading, maximum force holding, and linear unloading, each lasting 0.1 s. The maximum force was set to 1.5 mN.

The elastic properties were evaluated from the unloading segment of the force-displacement curve using the Oliver and Pharr theory [14], and the reduced modulus E_r was determined as

$$E_r = \frac{S\sqrt{\pi}}{2\beta\sqrt{A_c}}, \tag{1}$$

where A_c is the tip projected contact area, S represents the elastic unloading stiffness, and β is the tip geometry correction factor ($\beta = 1.034$ for a Berkovich tip). The reduced modulus combines the elastic stiffness of both the nanoindentation tip and the material. The Young's modulus, E, of the (isotropic) material can then be calculated using the following equation:

$$\frac{1}{E_r} = \frac{1-\nu^2}{E} + \frac{1-\nu_i^2}{E_i}, \tag{2}$$

where E_i and ν_i represent the Young's modulus and Poisson's ratio of the nanoindentation tip, respectively. For a diamond tip, the constants are assumed to be $E_i = 1141$ GPa and $\nu_i = 0.07$. ν denotes the Poisson's ratio of the sample, which was assumed to be 0.2 [15].

3. Results and discussion

In Figure 1, a typical example of a Young's modulus map measured by XPM is shown. A large range of E values, from 10 to 130 GPa were measured and based on the mechanical response and chemical composition, five different phases (residual clinker, Portlandite, inner product, outer product, low stiffness phase) were recognized [12]. The first phase consists of residual clinker with E values ranging from 50 GPa to 130 GPa. The second phase composed of Portlandite crystals where E are typically measured in the range of 36–43 GPa. Additionally, two phases based on C–S–H gel varying mainly in density of hydrates, were identified. The inner product, created primarily around residual clinker (E = 26–38 GPa) and outer product, more porous phase connecting the rest of the hydrates (E = 19–26 GPa). The last, low stiffness phase was mostly affected by larger pores with $E < 15$ GPa [15, 16]. The typical load–displacement curves of these phases are shown in Figure 2.

In the next step, all 4840 indents were merged together, and frequency density plots were created for

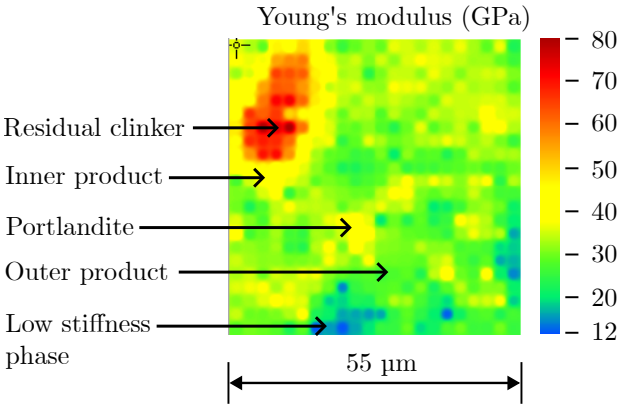

FIGURE 1. An example of a Young's modulus map obtained using XPM for the 76-IR sample.

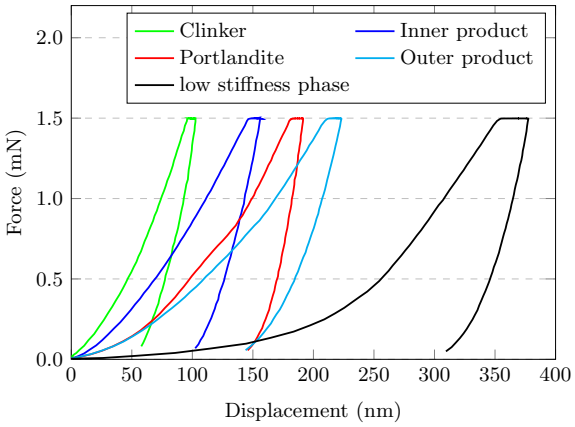

FIGURE 2. An example of typical force-displacement curves of main phases measured for the 76-IR sample.

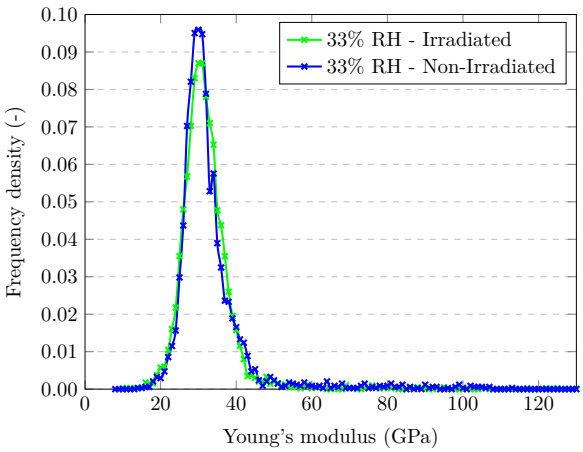

FIGURE 3. A typical example of frequency plots of Young's modulus for irradiated and non-irradiated samples stored at 33 % RH.

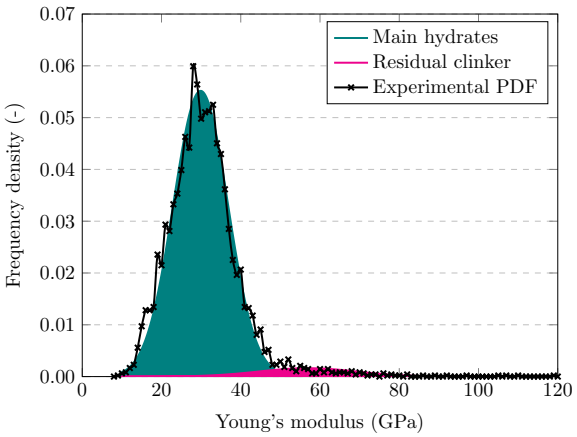

FIGURE 4. An example of statistical deconvolution of Young's modulus for the 76-IR sample.

each sample. An example of these plots is shown in Figure 3 for samples stored at 33 % RH. It is evident that the main peak is predominantly created by the main hydration products, including inner and outer products and Portlandite. This behavior was similar for all samples, with only a shift in the main peak being observable. Thus, it was decided not to separate the mechanical response into the main five phases but instead into two phases: one created by the main hydrates and the other by residual clinker, using a statistical deconvolution method, which assigns Gaussian distribution for each phase, as shown in Figure 4 for 76-IR sample. More details of the method can be found in [15, 16]. Based on these results, the micro-mechanical behavior between irradiated and non-irradiated samples was analyzed and is summarized in Figure 5.

The first group consists of samples stored at medium RHs (33 %, 76 %). The results show negligible differences between irradiated and non-irradiated samples, suggesting that the water loss caused by radiolysis is most likely counterbalanced by the RH conditions in the container. These findings are in accordance with other studies and apply to total gamma doses in the range of 0.257–15 MGy [5, 6, 10].

The second group consists of samples stored at low RH (11 %), which showed an increase in E by 9.5 % for non-irradiated samples and by 19.9 % for irradiated samples compared to those stored at medium RHs. This increase is attributed to drying shrinkage leading to the densification and compaction of C–S–H globules [17, 18]. The effect is even more pronounced in irradiated samples, where water radiolysis likely removes water from the interlayer space, further enhancing the densification and compaction effect. The increase of irradiated sample was measured as 9.3 %. The increase in irradiated samples aligns with other studies conducted at 11 % RH [8, 10]. However, the increase is much smaller compared to our previous study [10], where a 24.8 % increase was measured for samples irradiated with a significantly lower dose of 2.88 MGy. The main reason for this difference lies in the total hydration times of the samples; in the previous study, the samples were hydrated for only 4 weeks, compared to the well-matured samples that were hydrated for 1.5 years in the current study. This suggests that the degree of hydration at the beginning of irradiation has a significant effect on the

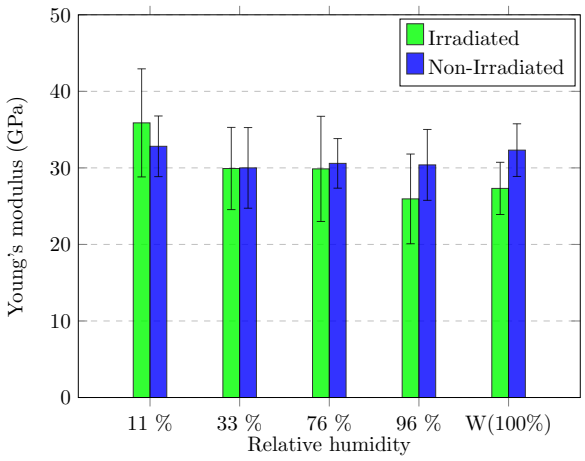

Figure 5. Summary of Young's modulus results of main hydrates for irradiated and non-irradiated samples stored at different RH levels.

overall changes due to irradiation.

The increase in irradiated samples aligns with other studies conducted at 11 % RH [8, 10]. Additionally, it should be noted that the local increase in E is accompanied by micro-cracking of the samples, leading to a decrease in mechanical properties at larger scales [10].

The third group consists of samples stored at high RHs (96 %, water–100 %). The mechanical properties of this group showed a significant decrease in E by 14.6 % (96 % RH) and 15.5 % (water), indicating the most negative effect and deterioration of the samples due to irradiation. Similar finding were also reported by Němeček et al. [10] for 28 days old samples irradiated with dose of 2.88 MGy. This deterioration is likely due to water radiolysis, although the exact mechanism is still unknown. Further analyses, such as X-ray diffraction, thermogravimetry, and porosity measurements by mercury intrusion porosimetry, will be performed to detect changes in structure and chemical composition.

The second phase created by residual clinker is not affected by gamma radiation, as it does not impact the crystalline phase [1]. The measured differences in micro-mechanical properties are primarily attributed to the dimensions of the clinker, which are embedded in the surrounding compliant cement matrix.

4. Conclusions

In this paper, the nanomechanical properties of ordinary cement paste exposed to different RHs and gamma radiation (total dose of 13.82 MGy) were investigated. Based on the different RH levels, the following conclusions were drawn:

- Samples irradiated at low RH (11 %) showed an increase in the Young's modulus by 9.3 %. This increase is attributed to the combination of water radiolysis and drying, possibly due to water removal from the interlayer space and compaction of the C–S–H phases.
- Samples irradiated at medium RHs (33 %, 76 %) showed almost identical nanomechanical properties, suggesting that samples in these conditions withstand gamma radiation best.
- Samples at high RHs showed a decrease of Young's modulus by 14.6 % (96 % RH) and 15.5 % (water), indicating that samples at high RH perform worst during gamma irradiation.

Future research should complement these findings with additional analyses detecting changes in porosity and chemical composition.

Acknowledgements

This work was financially supported by the project of the Czech Science Foundation grant number 23-05435S.

The presented results were obtained using the CICRR infrastructure, which is financially supported by the Ministry of Education and Culture – project LM2023041.

References

[1] T. Rosseel, I. Maruyama, Y. Le Pape, et al. Review of the current state of knowledge on the effects of radiation on concrete. *Journal of Advanced Concrete Technology* **14**(7):368–383, 2016. https://doi.org/10.3151/jact.14.368

[2] H. K. Hilsdorf, J. Kropp, H. J. Koch. The effects of nuclear radiation on the mechanical properties of concrete. *Special Publication* **55**:223–254, 1978.

[3] K. G. Field, I. Remec, Y. L. Pape. Radiation effects in concrete for nuclear power plants – Part I: Quantification of radiation exposure and radiation effects. *Nuclear Engineering and Design* **282**:126–143, 2015. https://doi.org/10.1016/j.nucengdes.2014.10.003

[4] P. Bouniol, A. Aspart. Disappearance of oxygen in concrete under irradiation: the role of peroxides in radiolysis. *Cement and Concrete Research* **28**(11):1669–1681, 1998. https://doi.org/10.1016/S0008-8846(98)00138-0

[5] Y. Khmurovska, P. Štemberk, S. Sikorin, et al. Effects of gamma-ray irradiation on hardened cement mortar. *International Journal of Concrete Structures and Materials* **15**(1):1–14, 2021. https://doi.org/10.1186/s40069-020-00452-7

[6] B. Hilloulin, M. Robira, A. Loukili. Coupling statistical indentation and microscopy to evaluate micromechanical properties of materials: Application to viscoelastic behavior of irradiated mortars. *Cement and Concrete Composites* **94**:153–165, 2018. https://doi.org/10.1016/j.cemconcomp.2018.09.008

[7] W. Hunnicutt, E. T. Rodriguez, P. Mondal, Y. Le Pape. Examination of gamma-irradiated calcium silicate hydrates. Part II: Mechanical properties. *Journal of Advanced Concrete Technology* **18**(10):558–570, 2020. https://doi.org/10.3151/jact.18.558

[8] A. Baral, E. T. Rodriguez, W. A. Hunnicutt, et al. Ultra-high gamma irradiation of calcium silicate hydrates: Impact on mechanical properties, nanostructure, and atomic environments. *Cement and Concrete Research* **158**:106855, 2022. https://doi.org/10.1016/j.cemconres.2022.106855

[9] O. Kontani, S. Sawada, I. Maruyama, et al. Evaluation of irradiation effects on concrete structure: Gamma-ray irradiation tests on cement paste. In *ASME Power Conference*, vol. 56062, p. V002T07A002. American Society of Mechanical Engineers, 2013.

[10] J. Němeček, P. Trávníček, M. Keppert, et al. Nanomechanical analysis of Gamma-irradiated cement paste exposed to different humidities. *Construction and Building Materials* **393**:131969, 2023. https://doi.org/10.1016/j.conbuildmat.2023.131969

[11] D. P. Bentz. CEMHYD3D: A three-dimensional cement hydration and microstructure development modeling package, Version 3.0. [2024-06-26]. https://www.nist.gov/services-resources/software/cemhyd3d

[12] J. Němeček, J. Lukeš, J. Němeček. High-speed mechanical mapping of blended cement pastes and its comparison with standard modes of nanoindentation. *Materials Today Communications* **23**:100806, 2020. https://doi.org/10.1016/j.mtcomm.2019.100806

[13] P. Sudharshan Phani, W. C. Oliver. A critical assessment of the effect of indentation spacing on the measurement of hardness and modulus using instrumented indentation testing. *Materials & Design* **164**:107563, 2019. https://doi.org/10.1016/j.matdes.2018.107563

[14] W. C. Oliver, G. M. Pharr. An improved technique for determining hardness and elastic modulus using load and displacement sensing indentation experiments. *Journal of materials research* **7**(6):1564–1583, 1992. https://doi.org/10.1557/JMR.1992.1564

[15] G. Constantinides, F.-J. Ulm. The nanogranular nature of C–S–H. *Journal of the Mechanics and Physics of Solids* **55**(1):64–90, 2007. https://doi.org/10.1016/j.jmps.2006.06.003

[16] G. Constantinides, F.-J. Ulm. The effect of two types of CSH on the elasticity of cement-based materials: Results from nanoindentation and micromechanical modeling. *Cement and concrete research* **34**(1):67–80, 2004. https://doi.org/10.1016/S0008-8846(03)00230-8

[17] J. Němeček, J. Maňák, J. Němeček, T. Krejčí. Effect of vacuum and Focused Ion Beam generated heat on fracture properties of hydrated cement paste. *Cement and Concrete Composites* **100**:139–149, 2019. https://doi.org/10.1016/j.cemconcomp.2019.03.027

[18] P. Suwanmaneechot, A. Aili, I. Maruyama. Creep behavior of C-S-H under different drying relative humidities: Interpretation of microindentation tests and sorption measurements by multi-scale analysis. *Cement and Concrete Research* **132**:106036, 2020. https://doi.org/10.1016/j.cemconres.2020.106036